

## Particle Transport and Electron Density Relaxation due to Stochastic Magnetic Fields in the MST Reversed Field Pinch

W.X. Ding<sup>1</sup>, D.L. Brower<sup>1</sup>, W. Bergerson<sup>1</sup>, G. Fiksel<sup>2</sup>, D. J. Den Hartog<sup>2</sup>, V. Mirnov, S.C. Prager<sup>2</sup>, J.S. Sarff<sup>2</sup>, T. Yates<sup>1</sup>

<sup>1</sup>University of California, Los Angeles, California 90095 USA

<sup>2</sup>University of Wisconsin-Madison, Madison, Wisconsin 53706 USA

e-mail: [wding@ucla.edu](mailto:wding@ucla.edu)

**Abstract:** Magnetic field fluctuation-induced particle transport and its divergence has been directly measured, for the first time, in the core of a high-temperature plasma. The measured convective electron particle flux, associated with correlated product of density and magnetic field fluctuations, can account for density relaxation during a magnetic reconnection event.

### 1. Introduction

Particle transport and its effect on the plasma density distribution remains an important, unresolved issue in magnetic fusion plasmas [1]. Fluctuating magnetic fields can arise from global tearing instabilities that often underlie the sawtooth oscillation [2] and lead to plasma relaxation [3]. Furthermore, magnetic fluctuations are also generated by energetic particles associated with non-inductive heating (NBI, ICRF) or inevitably generated intrinsically in burning plasmas by alpha particles. These fluctuations include various Alfvénic modes and energetic particle driven modes [4]. Conversely, stochastic magnetic fields have also been externally imposed (resonant magnetic perturbation) to mitigate the effect of edge localized modes (ELMs) by locally enhancing edge transport in Tokamaks [5]. Basic understanding of magnetic fluctuation-driven particle transport processes is thus of great interest and possibly critical to ELM control and fast particle losses in ITER. Progress to date is largely limited by the lack of direct measurements of the magnetic fluctuation-induced particle flux in hot plasmas.

The evolution of electron density is simply governed by particle balance

$$\frac{\partial n_e}{\partial t} + \nabla \cdot \Gamma_{r,e}^T = S_e, \quad (1)$$

where  $S_e = k_i n_0 n_e$  is ionization source ( $k_i$  ionization rate,  $n_0$  neutral density),  $\Gamma_{r,e}^T$  is fluctuation-induced transport flux as classical collision transport is negligible for high-temperature plasmas. The above relation indicates that density relaxation ( $\frac{\partial n_e}{\partial t} < 0$ ) can only arise from particle transport since  $S_e \geq 0$ . Measurement of particle flux induced by various fluctuations is critically important to understanding density relaxation.

Fluctuation-induced particle transport is traditionally classified as either electrostatic or magnetic in origin even though fluctuations are electromagnetic in general [1]. The total radial particle flux driven by fluctuations is given by [1,6]

$$\Gamma_{r,\alpha}^T = \frac{\langle \delta n \delta E_{\perp} \rangle}{B} + \frac{\langle \delta \Gamma_{\parallel,\alpha} \delta b_r \rangle}{B}. \quad (2)$$

The first term on the right hand side results from electrostatic fluctuations where  $\delta n$  and  $\delta E_{\perp}$  are density and perpendicular electric field fluctuations, respectively. The second term arises from magnetic fluctuations where  $\delta \Gamma_{\parallel,\alpha}$  is the fluctuating flux parallel to the magnetic field  $\bar{B}$  for species  $\alpha$  (electron or ion), and  $\delta b_r$  is the radial magnetic field fluctuation. Brackets  $\langle \dots \rangle$  denote a magnetic flux surface average. It is evident from the Eq. (2), that the magnetic fluctuation-induced particle flux depends on the species (electron or ion) while the electrostatic fluctuation-induced particle flux is intrinsically ambipolar. Fluctuating parallel flux arises from density and parallel velocity fluctuations according to the relation  $\delta \Gamma_{\parallel,\alpha} = V_{\parallel,\alpha} \delta n + n \delta V_{\parallel,\alpha}$ . Therefore, we can write the magnetic fluctuation-induced particle flux as the sum of two terms

$$\frac{\langle \delta \Gamma_{\parallel,\alpha} \delta b_r \rangle}{B} = V_{\parallel,\alpha} \frac{\langle \delta n \delta b_r \rangle}{B} + n \frac{\langle \delta V_{\parallel,\alpha} \delta b_r \rangle}{B}, \quad (3)$$

where  $V_{\parallel}$  ( $\delta V_{\parallel}$ ) is parallel equilibrium (fluctuating) velocity. The first term on the right hand side of Eq.(3) is the convective particle flux ( $\Gamma_{r,\alpha}^C$ ) while the second term can be referred to as a ‘‘pinch’’ term ( $\Gamma_{r,\alpha}^P$ ), which can be directed either inward or outward. Particle flux depends upon density fluctuations, parallel velocity fluctuations and their phase relation with radial magnetic field fluctuations.

In this paper, we report the first measurements of stochastic magnetic field driven convective electron particle flux in the high-temperature core of the MST reversed field pinch (RFP). Measurements focus on the sawtooth crash where stochastic magnetic fields resulting from tearing reconnection are strongest. Direct, nonperturbing measurements of the magnetic fluctuation-induced particle flux are made using a newly developed differential interferometer in combination with a fast Faraday rotation diagnostic. Measurements show that convective electron particle flux from stochastic magnetic field can account for the equilibrium density change in the core. The electron particle flux primarily arises from electron density fluctuations while ion particle flux arises from parallel ion velocity fluctuations.

## 2. Experimental Measurement

Measurements reported herein were carried out on the MST RFP [7] whose major radius  $R_0=1.5$  m, minor radius  $a=0.52$  m, discharge current 350~400 kA, line-averaged electron density  $\bar{n}_e \sim 1 \times 10^{19} m^{-3}$ , electron temperature  $T_e \sim T_i \sim 300 eV$ . Electron ionization rate  $k_i \approx 3.0 \times 10^{-14} m^3/s$ , neutral particle density in the core  $(2.0 - 4.0) \times 10^{15} m^{-3}$  measured by  $H_{\alpha}$  emission. Electron mean and fluctuating density are measured by interferometry [8], while the electron density gradient and fluctuating density gradient are obtained from differential interferometry [9]. Equilibrium and fluctuating magnetic fields are measured by a fast ( $t \sim 4 \mu s$ ) Faraday rotation diagnostic where 11-chords (chord separation  $\sim 8$  cm) probe the plasma cross section vertically [10,11]. Equilibrium magnetic field strength on the magnetic axis is measured to be 0.3~0.4 T and equilibrium current density is approximately 2

MA/m<sup>2</sup>. MST discharges display a sawtooth cycle in many parameters and measured quantities are ensemble (flux-surface) averaged over these reproducible sawtooth events.

Equilibrium electron density profile evolution during a sawtooth cycle for typical MST discharges without current profile control are shown in Fig.1 [8]. Density profile relaxation occurs in  $\sim 200 \mu\text{s}$ , much faster than classical collision time. The sawtooth is associated with magnetic reconnection driven by resistive tearing instabilities. Density relaxation is accompanied by mean current density relaxation as shown in Fig.2(a), where current density at the magnetic axis drops  $\sim 25\%$ . Current density relaxation is caused by Hall dynamo which is the correlated product of parallel current density and radial magnetic fluctuations [12].

Electron mean velocity,  $V_{\parallel,e} \approx \frac{J_{\parallel}}{n_e e}$ , is inferred from current density and electron density

measurement [Fig.2(b)] since electron motion dominates parallel current. Electron mean velocity does not show significant change at sawtooth crash, as shown in Fig.2(c). Magnetic fluctuation-induced anomalous particle flux is believed necessary to explain density relaxation since tearing mode driven magnetic reconnection is strongest at sawtooth crash.

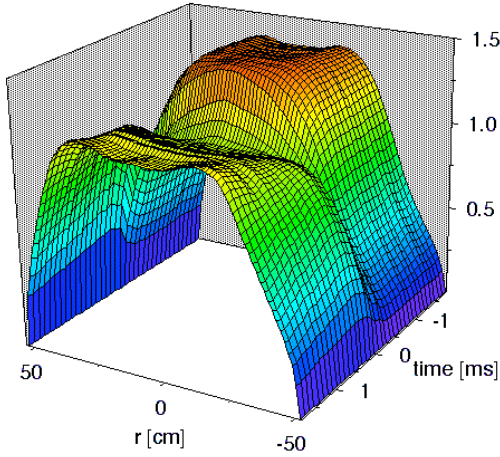


Fig. 1. Density relaxation during sawtooth crash which occurs at  $t=0$ . Vertical axis is density ( $\times 10^{13} \text{ cm}^{-3}$ ).

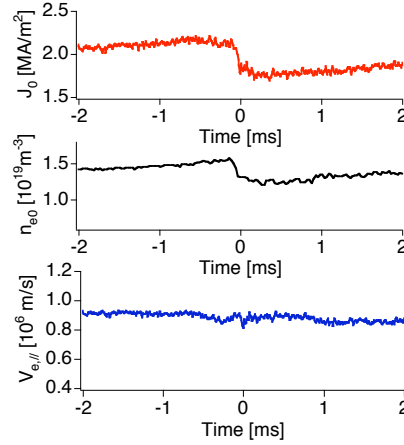


Fig. 2. Current density, electron density and parallel electron velocity over a sawtooth cycle.

In order to quantitatively determine the role of magnetic fluctuation-induced particle flux on the mean density profile, measurement of the particle flux divergence is required according to Eq.(1). We will initially focus on the convective part which arises from density fluctuations.

In cylindrical coordinates, the expression for  $\nabla \cdot \Gamma_{r,\alpha}^C$  can be simplified since measurements show that parallel electron velocity, mean magnetic and radial magnetic fluctuation are flat in the core. Therefore, we can write

$$\nabla \cdot \Gamma_{r,\alpha}^C = \frac{1}{r} \frac{\partial}{\partial r} (r \Gamma_{r,\alpha}^C) = \frac{V_{\parallel,e}}{B} \left( \left\langle \frac{\partial \delta n}{\partial r} \delta b_r \right\rangle + \left\langle \frac{\delta n}{r} \delta b_r \right\rangle \right) \approx 2 \frac{V_{\parallel,e}}{B} \left\langle \frac{\partial \delta n}{\partial r} \delta b_r \right\rangle. \quad \text{Note that}$$

$\delta n = \delta n(0) + r \frac{\partial}{\partial r} \delta n(0)$  near  $r=0$  and  $\delta n(0)=0$ . Measurements of the particle flux and its

divergence require measurement of (1) local density fluctuation and its derivative,  $\delta n$ ,  $\frac{\partial}{\partial r} \delta n$ ,

(2) magnetic field fluctuation  $\delta b_r$ , and (3) their correlation,  $\langle \delta n \delta b_r \rangle$ . In the following, measurement of each fluctuating quantity is described.

First, density fluctuations are measured using interferometry and differential interferometry techniques. In general, density fluctuations can be written as  $\tilde{n} = \sum_{m,n} \tilde{n}_{m,n}(r) \cos(m\theta + n\phi + \Delta(r))$  where  $m, n, \Delta$  are poloidal and toroidal mode number and phase, respectively. In MST, the dominant modes have  $m=1$  nature and the fluctuating phase measured by interferometry is given by  $\delta\phi(x) = r_e \lambda \int \delta n_{m=1}(r) \cos(\theta) dz$ , where  $r_e$  is electron classical radius,  $\lambda$  is laser wavelength,  $\cos\theta = \frac{x}{r}$  is a geometrical weighting factor, and  $x$  is the impact parameter. For chords close to the magnetic axis, the relation between phase fluctuation and density fluctuation can be simply written as

$$\delta n(r) \approx \delta\phi(x) \frac{1}{r_e \lambda L} \Big|_{x=r \rightarrow 0}. \quad (4)$$

Density fluctuation gradient is determined by differential interferometry which measures the phase difference between adjacent, closely-spaced ( $\Delta x \sim 1$  mm) chords. Differential interferometry provides a line-integrated density gradient measurement,  $\frac{\partial}{\partial x} \phi(x)$ . However, upon taking the first spatial derivative of line-integrated density we find  $\frac{\partial \phi(x)}{\partial x} = r_e \lambda \int \frac{\partial n(r)}{\partial r} \frac{\partial r}{\partial x} dz = r_e \lambda \int \frac{\partial n(r)}{\partial r} \cos(\theta) dz$ , where the cosine term is the same geometrical weighting factor described earlier. As  $x \rightarrow 0$ , the weighting factor narrows, approaching a delta function, thereby providing spatial resolution [9]. For small impact parameter  $x$ , differential interferometry essentially provides a localized measurement of the density gradient and density gradient fluctuations. Similar to Eq(4), we find

$$\frac{\partial}{\partial r} n(r) \approx \frac{\partial}{\partial x} \phi(x) \frac{1}{r_e \lambda L} \Big|_{x=r \rightarrow 0}, \quad (5)$$

which indicates the differential phase (or its fluctuation) is proportional to the local density gradient (or its fluctuation) for measurements made near the magnetic axis. This approximation provides the great convenience of being able to directly determine the local particle flux, in the plasma core, without performing any Abel inversion of the line integrated density measurements.

Measured electron density fluctuations and electron density gradient fluctuations at  $r/a=0.11$  exhibit a significant surge at the sawtooth crash as shown in Fig. 3. Density fluctuation amplitude away from the crash is approximately 0.15%, reaching 1% at  $t=0$ . Likewise, the density fluctuation gradient is nearly tripled at the crash. This is qualitatively consistent with the observation that maximum density relaxation occurs at a sawtooth crash, suggesting that large density fluctuations contribute to density relaxation.

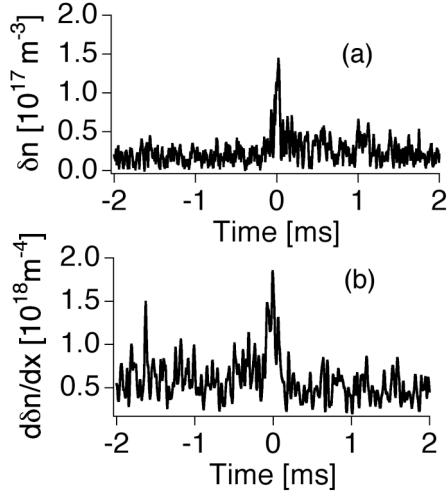


Fig. 3 (a) Electron density and (b) density gradient fluctuations during the sawtooth cycle at  $r/a=0.11$ . Sawtooth crash occurs at  $t=0$ .

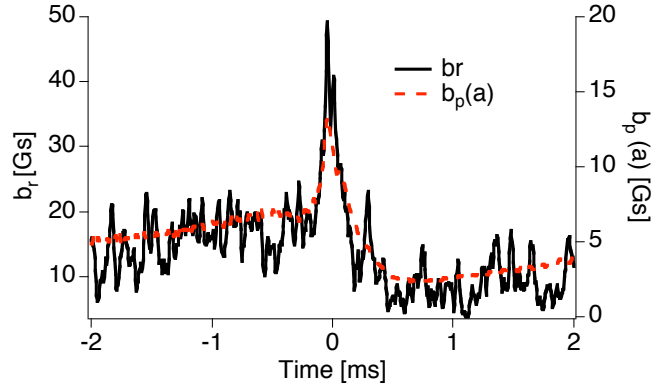


Figure 4. Line-averaged radial magnetic field fluctuation (solid) and edge poloidal magnetic field fluctuation (dashed) amplitudes during sawtooth cycle. Sawtooth crash occurs at  $t=0$ .

Second, radial magnetic field fluctuations can be obtained by measuring fluctuating components of Faraday rotation. Fluctuations in Faraday rotation can arise either from density fluctuation or magnetic fluctuations since Faraday rotation effect is a measure of product of density and magnetic field along a viewing line, *i.e.*  $\delta\Psi = c_F \int (n\delta B_z dz + \delta n B_z) dz$ , where  $c_F = 0.4889 \times 10^{-19} m^2 / T$  is a constant. It has previously been established that magnetic fluctuations dominate chords close to the magnetic axis [11,12] where  $\delta B_z$  reduces to  $\delta b_r$ . Therefore, for chords at small impact parameter, we have  $\delta\Psi = c_F \int n \delta b_r dz$ .

Measured line-averaged radial magnetic field fluctuations for the dominant core-resonant mode ( $m=1, n=6$ ), at frequency  $\sim 15-20$  kHz, through a sawtooth cycle are shown in Fig. 4. Maximum amplitude occurs at the crash. The poloidal magnetic fluctuation amplitude measured at the wall is also plotted in Fig.4, as a dashed line. Radial magnetic field fluctuations have similar dynamics as to poloidal magnetic field fluctuations as is expected for a global tearing mode. The local radial magnetic fluctuation profile is found by numerically fitting experimental data as described in earlier work [12,13]. In the core, radial magnetic field fluctuation amplitude in the core is approximately three times the poloidal magnetic field at the wall,  $\delta b_r(r) \sim 3 \times \delta b_\theta(a)$  for these conditions.

Measured phase between line-integrated radial and poloidal magnetic fluctuations at wall over sawtooth cycle is nearly constant and equal to  $-\pi/2$ , as shown in Fig.5. A  $\pi/2$  phase shift between radial and poloidal magnetic fluctuations at wall is required by plasma boundary condition where  $\nabla \cdot \delta B|_{r=a} = 0$ . Constant phase over minor radius for  $\delta b_r$ , predicted by tearing mode theory and MHD computation, has been verified by probe measurement in the region where the temperature is lower ( $r/a > 0.6$ ). Core measurement of radial magnetic

fluctuations implies that constant phase for radial magnetic fluctuation is also valid in the region  $r/a < 0.6$ .

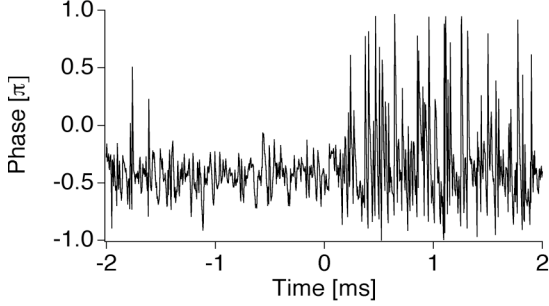


Fig.5 Phase between line-integrated radial magnetic fluctuations and poloidal magnetic fluctuations at wall.

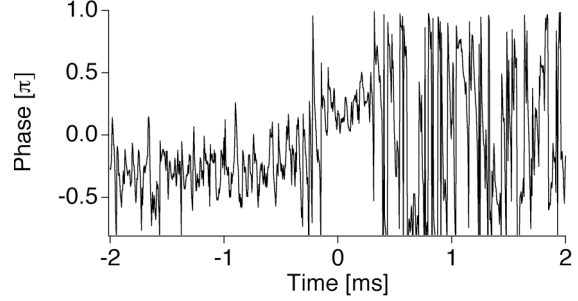


Fig.6 The phase between density fluctuation and radial magnetic field fluctuation changes from nearly  $\pi/2$  (away sawtooth) to 0 (at sawtooth).

Finally, the phase between  $\delta n$  (or  $\frac{\partial}{\partial r} \delta n$ ) and  $\delta b_r$  can be obtained by ensemble averaging. In MST, rotation of the low- $n$  magnetic modes transfers their spatial structure in the plasma frame into a temporal evolution in the laboratory frame. Since the magnetic modes are global, for convenience we correlate  $\delta n$  (or  $\frac{\partial \delta n}{\partial r}$ ) to a specific helical magnetic mode which is spatially Fourier decomposed from 32 wall-mounted magnetic coils. After averaging over an ensemble of similar events ( $\sim 400$  events are used), we can determine the phase between  $\delta n$  (or  $\frac{\partial \delta n}{\partial r}$ ) and  $\delta b_r$  for the specified mode. For tearing modes, the radial magnetic perturbation has a constant phase over minor radius as discussed above. Therefore, we correlate core density gradient fluctuations to poloidal magnetic field fluctuations measured at the wall to determine the phase.

The measured phase between density fluctuations and radial magnetic field fluctuations for mode with helicity  $m/n=1/6$  is illustrated in Fig.6. During sawtooth cycle, this phase varies from nearly  $-\pi/2$  to  $\pi/2$ . This indicates that particle flux ( $\Gamma_{r,e}^c \sim |\delta n| |\delta b_r| \cos \Delta_{nb_r}$ ) has a significant change at the sawtooth crash where the maximum flux occurs since  $\Delta_{nb_r} \approx 0$  and the fluctuation amplitudes peaks. By combining measurements of density fluctuations, density gradient fluctuations, radial magnetic fluctuations and their respective phase, a direct, nonperturbing measurement of the convective magnetic fluctuation-induced electron particle flux is obtained as shown in Fig. 7(a). Here contributions from the dominant core resonant modes ( $m=1, n=6,7,8,9$ ) to the convective particle flux are included. The particle flux surges, reaching  $\sim 1.0 \times 10^{21} \text{ m}^{-2} \text{ s}^{-1}$ , at a sawtooth crash. This corresponds to the same time the core density collapse occurs. Positive sign of flux indicates outward transport. Divergence of particle flux also increases significantly as shown in Fig. 7(b), reaching  $2.0 \times 10^{22} \text{ m}^{-3} \text{ s}^{-1}$ .

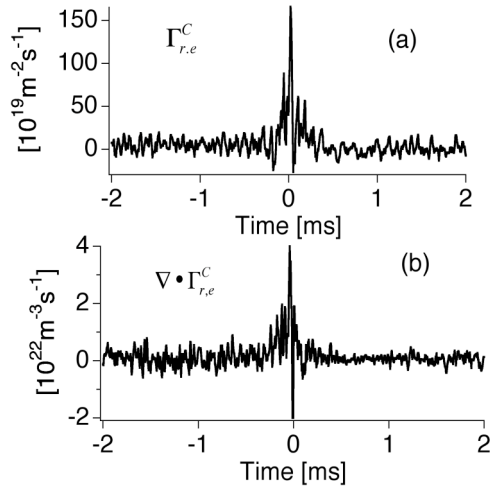


Fig. 7. (a) Convective particle flux and (b) its divergence at  $r/a=0.11$ , for the dominant core resonant modes.

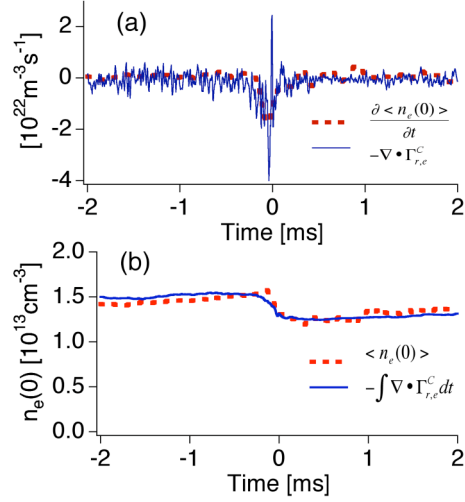


Fig. 8. (a) Time change rate of electron density (dashed) is balanced by electron particle flux divergence (solid), and (b) time-integrated results at  $r/a=0.11$ .

The fast density profile relaxation at a sawtooth crash (see Fig.1) implies a surge of  $dn/dt$ , as indicated in Fig. 8(a) [dashed-red]. The measured  $-\nabla \cdot \Gamma_{r,e}^c$  [solid-blue] shows a similar surge, reaching  $2.0 \times 10^{22} m^{-3} s^{-1}$ , essentially balancing the density change within experimental errors. One can integrate these two curves over time to directly compare the density change and particle flux as shown in Fig.8 (b). This clearly illustrates that stochastic magnetic field driven particle flux (convective part) can account for the observed density change at a sawtooth crash. Away from sawtooth crash, the measured magnetic fluctuation-induced particle flux is approximately  $(1.0 - 1.5) \times 10^{20} m^{-2} s^{-1}$ , comparable to particle flux obtained from particle balance for standard plasma discharges where no current profile shaping is applied [8].

Similarly, ion convective flux  $\Gamma_{r,i}^C = 2 \frac{V_{||,i}}{B} \langle \delta n \delta b_r \rangle$  can be obtained experimentally where  $V_{||,i}$  is ion parallel velocity. Since ion parallel velocity ( $\sim 10^4$  m/s) is much less than electron parallel velocity ( $10^6$  m/s),  $\Gamma_{r,i}^C \ll \Gamma_{r,e}^C$ . However, the difference between ion flux and electron flux (charge flux  $\Gamma_q$  due to magnetic fluctuation) has been measured to be small ( $\Gamma_q = \Gamma_{r,i} - \Gamma_{r,e} \approx 10^{-2} \Gamma_{r,e}$ ) [14], that is  $\Gamma_{r,i} \approx \Gamma_{r,e}$ . Therefore the ion flux must arise from the pinch term ( $\Gamma_{r,i} = \Gamma_{r,i}^C + \Gamma_{r,i}^P \approx \Gamma_{r,i}^P = n \frac{\langle \delta V_{||,i} \delta b_r \rangle}{B}$ ), where parallel ion velocity fluctuations now play an important role in ion transport. Indeed, measured ion velocity fluctuations surge at the sawtooth crash and have strong correlation with radial magnetic field fluctuations in the core, also referred to as MHD dynamo [15]. It is interesting to note that the ion flux and electron flux originate from different mechanisms and plasma quasi-neutrality forces them to be comparable. This implies ion parallel velocity fluctuations could be coupled to electron mean velocity and density fluctuations via particle transport.

Since the electron convective particle flux can account for density relaxation, the total particle flux arising from all other mechanisms ( *i.e.* electrostatic fluctuations, electron pinch term and collisions) is small by implication. It should be noted that the measurement of convective electron flux by itself does not prove that each of the other mechanisms has to be small. However, electrostatic fluctuation-induced particle flux measurements, made by a Heavy Ion Beam Probe, were found to be negligible in the plasma core on MST [16]. Measurement of the other mechanisms awaits the development of new diagnostic techniques for high temperature plasmas.

In summary a direct measurement of magnetic fluctuation-induced convective particle flux and its divergence has been made, for the first time, in the core of a high-temperature plasma. The convective electron particle flux during a sawtooth crash associated with magnetic reconnection can account for density relaxation in the plasma interior. The difference between the electron and ion fluxes can also be measured and is found to be small (nonzero but less than 1% of the total flux), implying  $\Gamma_e \sim \Gamma_i$ , as expected from quasineutrality. Since the convective flux for ions is small due to small parallel velocity (compared to electrons), ion flux arises primarily from the pinch term. This implies the origin of ion particle flux is parallel ion velocity fluctuations correlated with radial magnetic fluctuations. In contrast, the electron flux results from electron density fluctuations correlated with radial magnetic fluctuations.

## Reference

- [1] P.C. Liewer, Nucl. Fusion, **25**, 543(1985).
- [2] A. B. Rechester and M. N. Rosenbluth, Phys. Rev. Letts. **40**, 38(1978).
- [3] S. Ortolani and D. D. Schnack, *Magnetohydrodynamics of Plasma Relaxation* (World Scientific, Singapore, 1993).
- [4] W.W. Heidbrink *et al.*, Phys. Fluids B **5**,2176(1993).
- [5] T.E. Evan, *et al*, Phys. Rev. Lett. **92**,235003 (2004); L.Zeng, *et al*, the *bulletin of 48<sup>th</sup> annual meeting of American Physical Society*, Philadelphia, PA, pp. 329, 2007.
- [6] S.C. Prager, Plasma Phys. and Controlled Fusion **32**, 903(1990).
- [7] R.N. Dexter, *et al.* , Fusion Technol. **19**, 131(1991).
- [8] N. E. Lanier *et al.* , Phys. of Plasmas **8**, 3402 (2001).
- [9] W.X. Ding, D.L. Brower, B.H. Deng and T.Yates, Rev. Sci. Instrum. **77**,10F105 (2006).
- [10] D.L.Brower, *et al.*, Phys. Rev. Lett. **88**,185005(2002).
- [11] W.X.Ding, *et al.*, Phys. Rev. Lett. **90**,035002(2003).
- [12] W.X.Ding, *et al.*, Physics of Plasmas **13**,112306(2006); W.X.Ding, *et al.*, Phys. Rev. Lett. **93**,045002(2004).
- [13] W.X. Ding *et al.* , Rev. Sci. Instrum. **75**, 3387(2004).
- [14] W.X. Ding, D.L. Brower, D. Craig, B.H. Deng, S.C. Prager, J.S. John and V. Svidzinski, Phys. Rev. Lett. **99**, 055004(2007); W.X. Ding, *et al.* Physics of Plasmas, **15**,055901 (2008).
- [15] D.J. Den Hartog, *et al*, Phys. Plasmas **6**, 1813(1999).
- [16] J. Lei, P.M. Schoch, D.R. Demers, U. Shah, K.A. Connor, J.K. Anderson, T.P.Crowley, Phys. Rev. Lett. **89**, 275001(2002).